Accepted Manuscript

Bifunctional $(Zn,Fe)_3O_4$ nanoparticles: Tuning their efficiency for potential application in reagentless glucose biosensors and magnetic hyperthermia

Miloš Ognjanović, Dalibor M. Stanković, Yue Ming, Hongguo Zhang, Boštjan Jančar, Biljana Dojčinović, Željko Prijović, Bratislav Antić

PII: S0925-8388(18)34068-4

DOI: https://doi.org/10.1016/j.jallcom.2018.10.369

Reference: JALCOM 48187

To appear in: *Journal of Alloys and Compounds*

Received Date: 4 September 2018

Revised Date: 8 October 2018

Accepted Date: 28 October 2018

Please cite this article as: Miloš. Ognjanović, D.M. Stanković, Y. Ming, H. Zhang, Boš. Jančar, B. Dojčinović, Ž. Prijović, B. Antić, Bifunctional $(Zn,Fe)_3O_4$ nanoparticles: Tuning their efficiency for potential application in reagentless glucose biosensors and magnetic hyperthermia, *Journal of Alloys and Compounds* (2018), doi: https://doi.org/10.1016/j.jallcom.2018.10.369.

Bifunctional $(Zn,Fe)_3O_4$ nanoparticles: Tuning their efficiency for potential application in reagentless glucose biosensors and magnetic hyperthermia

Miloš Ognjanović[1*], Dalibor M. Stanković[1,2], Yue Ming[3], Hongguo Zhang[3], Boštjan Jančar[4], Biljana Dojčinović[5], Željko Prijović[1] and Bratislav Antić[1]

[1]The Vinca Institute of Nuclear Sciences, University of Belgrade, POB 522, 11001 Belgrade, Serbia

[2]Innovation center of the Faculty of Chemistry, University of Belgrade, POB 522, 11001 Belgrade, Serbia

[3]College of Materials Science and Engineering, Beijing University of Technology, Pingleyuan 100, Chaoyang District, Beijing 100124, P. R. China

[4]Jožef Štefan Institute, Jamova 39, 1000 Ljubljana, Slovenia

[5]Institute of Chemistry, Technology and Metallurgy, University of Belgrade, Studentski trg 12-16, 11000 Belgrade, Serbia

**corresponding author*: Miloš Ognjanović, The Vinca Institute of Nuclear Sciences, University of Belgrade, POB 522, 11001 Belgrade, Serbia. Email: miloso@vin.bg.ac.rs Phone: 00381 11 3336829

Abstract

In a new approach based on a two-step procedure, co-precipitation method followed by hydrothermal treatment in a microwave field, Zn-substituted Fe_3O_4 nanoparticles ($Zn_xFe_{3-x}O_4$) were synthesized. Results of XRD, FT–IR and TEM analysis clearly demonstrate that nanoparticles were single phase, crystallizing in the spinel structure type (S.G. $Fd\bar{3}m$) with

crystallite size in the range of 2–20 nm, which strongly depends on Zn concentration. The produced nanoparticles were used for fabrication of modified carbon paste electrodes as a novel system for electrochemical non-enzymatic glucose detection. It was found that the increase of zinc concentration up to the value of $x = 0.56$ ($Zn_{0.56}Fe_{2.44}O_4$) of as-prepared nanoparticles was followed with an increase of a performance of the modified carbon paste electrode toward glucose detection. Linear working range from 0.1 to 2 mM was obtained with detection limit of 0.03 mM, and with fast response time (< 3 s). Proposed sensor was successfully applied for the determination of glucose level in real samples with satisfactory recovery. The synthesized zinc-ferrite samples were also tested as potential heating agents in magnetic hyperthermia. The heating ability (SAR value) increases with x value, reaching maximum for $x = 0.37$. This is correlated with changes of particle size and magnetic characteristics which strongly depend on Zn concentration.

Keywords: MW hydrothermal synthesis; Structural characterization; Carbon electrodes; Glucose sensor; Hyperthermia.

1. Introduction

Nanostructure metal oxides crystallizing in the spinel structure type have been investigated intensively over the years and present a permanent interest due to their wide technological applications such as magnetic and optical materials [1–3], semiconductors [4], pigments [5], catalysts [6,7], or material for biomedical applications [8]. Among them, spinel ferrites with general formula $M^{2+}Fe_2O_4$ (M^{2+} = Fe^{2+}, Mg^{2+}, Zn^{2+}, Co^{2+}, Mn^{2+}, Ni^{2+}, *etc.*) are important class of materials both in nano and bulk form. Besides practical applications they attract scientists from fundamental point of view and serve as model systems in theoretical investigations. By partial

substitution of iron by 3d or 4f elements in $M^{2+}Fe_2O_4$, mixed ferrites are formed. Level of substitution can significantly modify physicochemical properties of parent compounds.

Magnetite nanoparticles are known as one of the most common compounds used for biomedical applications. They exhibit some promising properties such as biocompatibility [9] and low toxicity [10] in human body, possibility to transfer to superparamagnetic form by decreasing their particle size, and ease of synthesis process and surface treatment [11]. Currently, magnetite (Fe_3O_4) and maghemite (γ-Fe_2O_3) are the only two U.S. food and drug administration (FDA) approved magnetic materials that can be used in humans as iron deficiency therapeutics and as MRI contrasting agents [12].

On the other side, nano $ZnFe_2O_4$ is found to be one of the most interesting spinel systems because of its unique properties, photochemical stability, good visible-light response and favourable magnetism [13]. It has a mixed spinel structure $(Zn^{2+}_{1-\delta}\ Fe^{3+}_{\delta})_{Td}[Fe^{3+}_{2-\delta}\ Zn^{2+}_{\delta}]_{Oh}O^{2-}_4$ with cations Zn and Fe occupying both crystallographic sites, tetrahedral Td and octahedral Oh in $Fd\bar{3}m$ space group, and spinel type of structure. The "δ" denotes inversion degree and can have values from 1 for normal spinel and 0 for inversed one [14].

A plenty of synthetic methods have been proposed for preparing $ZnFe_2O_4$, Fe_3O_4 and mixed $Zn_xFe_{3-x}O_4$ such as coprecipitation [15], sol-gel method [16], electrochemical synthesis [17], reverse micelles [18], mechanical alloying [19], solvothermal method [20], chemical solution deposition [21] and so on. In recent years, the microwave-assisted hydrothermal synthesis has been intensively developed due to rapid heating, higher yield, faster kinetics, homogeneity of prepared samples compared with the conventional hydrothermal method [22,23], and successfully applied in preparation of ferrites such as Fe_3O_4 [24], $MgFe_2O_4$ [25], $CoFe_2O_4$ [26], $NiFe_2O_4$ [27], etc. One of the goals of this study was to find a quick, simple and cost-efficient

method for synthesis of $Zn_xFe_{3-x}O_4$ nanoparticles in broad Zn concentration range. Here, we report the two-step method for the preparation $Zn_xFe_{3-x}O_4$ nanoparticles. The produced nanoparticles were then used for fabrication of modified carbon paste electrodes which were further investigated for non-enzymatic electrochemical glucose detection. Also, the influence of Zn/Fe ratio on performance of the electrodes was investigated.

Glucose sensing devices have important applications in clinical diagnostic and food industry. Nowadays, most of commercial products are enzymatic glucose sensors due to being fast and reversible but they still suffer from lack of the stability because nature of enzymes which remains main problem with this type of sensors [28]. In recent years, much research is oriented on non-enzymatic glucose sensors to overcome the limitations such as stability and accuracy [29,30]. Electrochemical glucose sensors such as amperometric and potentiometric are frequently used techniques for continuous monitoring because of low cost, fast response time, selectivity, and wider sensing range [31,32]. By means of advanced fabrication techniques, various micro- and nano- structural materials such as noble metals (Au, Pt, Pd) [33–35], composite alloy metals (Ni-Cu, Pt-Au, Pt-Pb) [36–38], and various modified metal oxide nanoparticles (ZnO, Fe_3O_4) [39,40] have been recently employed in the preparation of electrodes for non-enzymatic glucose sensing, by improving biosensor activity, biocompatibility and chemical stability. Materials containing Zn in their structure, such as ZnO and different varieties of Zn materials, are nowadays widely investigated for the application as biological sensing devices, due to many favourable properties. Wide direct band gap (3.37 eV) and large exaction binding energy (60 meV) as well as their piezoelectric and semiconducting properties found significant application in different research areas including electrochemical sensors and biosensors [41]. Due to high ability and favourable reaction with oxygen these materials are one of best

promising materials in the field of sensors [42]. Herein, we have developed a new glucose flexible electrochemical sensor based on magnetic nanoparticles of zinc-ferrite for a rapid, simple and quantitative monitoring of glucose.

Magnetic hyperthermia (MH) is one of the most promising techniques in the treatment of malignant diseases. The most commonly used nanoparticles for magnetic hyperthermia are ferromagnetic or superparamagnetic Fe_3O_4 and γ-Fe_2O_3. Recently, the biggest challenge is to synthesize magnetic nanoparticles (MNPs) with high heating ability (expressed by specific absorption rate, SAR). Hence, the attention is focused on the synthesis of complex magnetic oxides where it is possible to tailor the properties and increase of the SAR by modifying physicochemical parameters of synthesis. It is well known that the particle size and composition are closely correlated with morphological and magnetic properties of MNPs, consequently, one of the aims of this work was to investigate the influence on heating ability by modifying Zn concentration in $Zn_xFe_{3-x}O_4$.

The main goals of this work were preparation of $Zn_xFe_{3-x}O_4$ nanoparticles and $Zn_xFe_{3-x}O_4$/carbon paste electrodes, fabrication and optimization of chemical composition of $Zn_xFe_{3-x}O_4$/carbon paste electrodes for enhanced reagentless detection of glucose and investigation of Zn concentration influence ($Zn_xFe_{3-x}O_4$) on heating efficiency in magnetic hyperthermia.

2. Material and methods

2.1.Chemicals

Iron(II) sulphate heptahydrate ($FeSO_4 \cdot 7H_2O$, ACS reagent, ≥99.0%), zinc chloride ($ZnCl_2$, p.a ≥98%), ammonium hydroxide solution (NH_4OH, ACS reagent, 28,0–30,0% NH_3 basis), carbon (glassy, spherical powder, 2-12 µm, 99,95%), citric acid ($C_6H_8O_7$, 99%) and mineral oil (light)

were purchased from Sigma Aldrich. Iron(III) chloride hexahydrate ($FeCl_3 \cdot 6H_2O$, ACS reagent, ≥ 99.0%) and sodium hydroxide (NaOH, reagent grade, ≥97.0%) were were purchased from Merck, Germany.

2.2.Synthesis of nanoparticles

All reagents were of analytical grade and were used as received without further purification. The synthesis of nanoparticles has been based on our previous work [43]. Here, the procedure was successfully applied to the preparation of Zn-ferrites with different amounts of Zn. The nanoparticles represented with formula unit $Zn_xFe_{3-x}O_4$ were prepared by two-step procedure, coprecipitation method at room temperature followed by hydrothermal treatment in microwave field at 100°C. Briefly, the iron and zinc salts were added to round bottom flask under a blanket of nitrogen and vigorous mechanical stirring. The nanoparticles were precipitated with NH_4OH for 1 hour dropwise, and transferred to the microwave reactor. The power of microwave irradiation was set between 0-1000 W, with a linear heating of mixture from room temperature to 100°C for 10 min. Vessels were quickly cooled in an air flow, and obtained black product was collected by external magnet and washed with demineralized water several times. Finally, the nanoparticles were dispersed in water. The synthesized samples were dried overnight at 60°C for further characterization.

2.3.Preparation of modified electrodes

The unmodified carbon paste electrode was prepared in a standard way, by mixing carbon powder and oil in an 80:20 ratios, followed with homogenizing by handle mixing. For the electrode a Teflon tube with inner diameter of 3 mm was used. Modified electrodes were

prepared by adding 5 wt % of synthesized $Zn_xFe_{3-x}O_4$ to the carbon powder and following the procedure for preparing the unmodified electrode.

2.4. Experimental techniques

The Zn and Fe contents in the $Zn_xFe_{3-x}O_4$ samples were determined using the inductively coupled plasma atomic emission spectroscopy (ICP-AES) performed on a Thermo Scientific iCAP 6500 Duo ICP system. The structure/microstructure of the samples was checked/determined using X-ray diffraction data. The data were collected with a SmartLab® X-ray diffractometer (Rigaku), using Cu Kα radiation (λ = 0.1542 nm). The experimental conditions were: a step size of 0.05^o and with exposition of 3 s per step in the 2θ ranging from 15^o to 70^o with divergent slit of 0.5 mm, operated at 40 kV and 30 mA. The morphology and the distribution of the particles were also investigated, with help of transmission electron microscope (TEM) JEM-2100 operated at 200 kV. Presence of organic molecules at the surface of the particles (capping agent) were checked by Fourier transform-infrared spectroscopy (FT-IR) in the region from 400 cm^{-1} to 4000 cm^{-1} using a Nicolet iS50 FT-IR, Thermo Fisher Scientific spectrophotometer equipped by Smart iTR attenuated total reflectance (ATR) sampling accessory, by fixing the samples on diamond plate. The background spectra were measured on a clean and dry diamond crystal.

Electrochemical measurements were performed using an electrochemical system CH Instruments. The cell (5 ml) consisted of a three-electrode system, carbon paste electrode or modified electrode as working electrode, an Ag/AgCl (saturated KCl) reference electrode and a Pt wire counter electrode. All potentials obtained in this study were reported vs. Ag/AgCl reference electrode at ambient temperature. pH values were measured with pH meter model Jenco Instruments Model No. 6071 (Taiwan), using a combined glass electrode.

2.5. Magnetic measurements

Magnetic properties were studied by means of Quantum Design MPMS XL SQUID (H_{max} = 70 kOe) and Quantum Design VersaLab VSM (H_{max} = 30 kOe). Different kinds of magnetic measurements were carried out. Magnetization *vs*. magnetic field curves were measured at 300 K between -30 kOe and 30 kOe. The saturation magnetization (Ms) was estimated by using the equation 1:

$$M = M_s\left(1 - \frac{a}{H} - \frac{b}{H^2}\right) \text{ for H tending to } \infty, \quad (1)$$

Magnetization vs. temperature were measured between 5 K and 300 K. The samples were cooled from ambient temperature to 5 K without field (ZFC) and after that the samples were cooled from room to 5K in small magnetic field (H = 100 Oe) (FC) with measure of magnetization.

Calorimetric measurements of SAR were performed by means of non-adiabatic experimental setup DM100 Series built by nanoScale Biomagnetic magnetic fluid hyperthermia measuring system. Kinetic (heating) curves were recorded under a magnetic field of 15.9 kA m^{-1} and two different frequencies (252 kHz and 577 kHz) for 120 s on water colloidal dispersions of the magnetic nanoparticles. Nanoparticles have been coated by intercalation process with citric acid ($C_6H_8O_7$) in order to get more stable suspension. Coating procedure was done by mixing NPs and citric acid in concertation of 0.6 mmol CA/g of nanoparticles at room temperature in ultrasonic bath for 30 min. After intercalation process with citric acid, all samples were stable in interval of few hours. The concentration of the colloidal dispersion was 3 mg ml^{-1} for all the samples. Temperature of the sample was monitored by optical fiber probe. Colloid temperature was kept below 65°C to minimize evaporation and prevent colloid destabilization. The SAR

values have been estimated by a linear curve fitting in the first 30 s of the heating curves (initial slope method). SAR is defined as the power dissipation per unit mass of iron (W/g).

3. Results and discussion

3.1. Structural and microstructural characterization

The Zn and Fe content in the $Zn_xFe_{3-x}O_4$ samples was determined using ICP-OES technique. The obtained results were slightly different from those targeted (Table 1 and Figure S1, Supplementary material). It seems that for higher x values ($x > 0.6$) some unreacted quantity of Zn salts remains in supernatant.

The diffraction patterns of the $Zn_xFe_{3-x}O_4$ (x = 0, 0.10, 0.20, 0.37, 0.56, 0.66 and 0.85) are shown in Figure 1a. The reflections for all samples appeared at approximately same positions as those of pure magnetite (x = 0). This indicates that all reflections could be indexed in the $Fd\bar{3}m$ (No. 227) space group of the cubic structure, suggesting that the samples have spinel structure (ICDD PDF #22-1012). The samples' mean crystallite size, determined by Sherrer's equation [44], decreases with the increase of zinc (x) amount, from 15.5 nm for Fe_3O_4 to 2.2 nm for $Zn_{0.85}Fe_{2.15}O_4$. It is worth noting that addition of Zn salts in solution suppress particle/crystallite size growth, Table 1. Final sample of the series doesn't have well-arranged crystal structure and lattice parameter couldn't be determined due to very broad reflections.

The value of lattice parameter (a) linearly increases Zn concentration, Table 1 and Figure 1b, corresponding to the Vegard rule [45]. This is a confirmation of replacement of iron by zinc in magnetite. The trend could be explained by considering the size of iconic radii of the metal ions. Zn^{2+} has bigger radius (0.74 Å), whereas $Fe^{2+}$and Fe^{3+} are smaller (0.61 Å and 0.49 Å) which

may induce in increase of the lattice parameter [46,47]. Considering that Td sites are smaller than the Oh ones, a higher occupancy of the Td sites by bigger metal cations will lead to the dilatation of the structure and, subsequently, to an increase of a lattice parameter. The shift of the (311) reflection peak to lower angles due to cell expansion is shown in the inset of Figure 1b. It is worth noting that *Liu et al*. also reported a similar effect of *x* on the length of the *α*-axis and the crystal size with the Zn contents below 0.4 and indicated that that *x* value might be an acceptable limit of forming the $Zn_xFe_{3-x}O_4$ crystal [48].

>>>Here Figure 1<<<

Table 1. Chemical composition of the samples according stoichiometric ratio of starting compound (targeted) and determined by ICP-OES. Lattice parameter *a*, crystallite size $<D_{XRD}>$ and particle size $<D_{TEM}>$ with polydispersity σ_{TEM} are shown.

Chemical composition (Targeted)	Chemical composition (ICP-OES)	$<D_{XRD}>$ (nm)	*a* (Å)	$<D_{TEM}>$ (nm)	σ_{TEM} (%)
Fe_3O_4	Fe_3O_4	15.5(3)	8.368(7)	19.8	26.1
$Zn_{0.1}Fe_{2.9}O_4$	$Zn_{0.10}Fe_{2.90}O_4$	13.6(5)	8.382(1)	17.8	26.5
$Zn_{0.2}Fe_{2.8}O_4$	$Zn_{0.20}Fe_{2.80}O_4$	11.9(6)	8.398(8)	15.2	26.6
$Zn_{0.4}Fe_{2.6}O_4$	$Zn_{0.37}Fe_{2.63}O_4$	10.3(8)	8.447(6)	12.8	24.5
$Zn_{0.6}Fe_{2.4}O_4$	$Zn_{0.56}Fe_{2.44}O_4$	5.0(8)	8.467(1)	8.3	28.7
$Zn_{0.8}Fe_{2.2}O_4$	$Zn_{0.66}Fe_{2.34}O_4$	4.7(9)	8.469(5)	8.0	29.2
$ZnFe_2O_4$	$Zn_{0.85}Fe_{2.15}O_4$	2.2(5)	-	4.1	23.3

An accurate description of particle size, size distribution and morphology were derived from a statistical analysis of more than 500 particles for each sample collected from different parts of the grid, as observed in TEM experiments (Figure 2). As can be seen from TEM images, particle with *x* from 0.0 to 0.56 behave as pseudo-spherical nanoparticles which undergoes log-normal size distribution. The average diameters of the nanoparticles ($<D_{TEM}>$) and polydispersity (σ_{TEM}) are listed in Table 1. It can be seen that the evaluated average particle size is comparable with crystallite size obtained from XRD which indicate that nanoparticles have high crystallinity and that they are monocrystals and free of defects. Crystallinity decreases with substitution with Zn^{2+}, and also particles change in shape from spherical to rounded cubic morphology (Figure S2). Additionally, it was found that the average diameter of nanoparticles decreases with increasing *x* from 0.0 to 0.56, and roughly remained constant value for $x = 0.66$ and $x = 0.85$. Low crystallinity of the sample with $x = 0.85$ is confirmed with TEM analysis also (Figure S2c).

>>>Here Figure 2<<<

FT-IR analysis (Figure S3) is useful technique to give us more information about the inorganic phase, Me–O (Me = Zn, Co, Mg) stretching modes of spinel ferrites falling in the fingerprint region (1500 cm^{-1} to 500 cm^{-1}). The metal–oxygen stretching vibrations of the Td and Oh sites are moving towards lower values for increasing zinc content, from 555 cm^{-1} for magnetite to 537 cm^{-1} $Zn_{0.56}Fe_{2.44}O_4$. Considering values previously reported in the literature for pure magnetite (570 cm^{-1}) and zinc ferrite (555 cm^{-1}) [49], this trend can be interpreted as a gradual substitution of Fe^{2+} by the Zn^{2+} inside of a spinel structure. In Figure S3b observed ν values are decreasing, going from magnetite to zinc ferrite with the exception of sample $Zn_{0.66}Fe_{2.34}O_4$. That may be attributed to cationic distribution because not all Zn ions lie on tetrahedral site but a mixed cationic distribution may exists depending on Zn/Fe ratio or due to other factor.

3.2. Magnetic characterization of $Zn_xFe_{3-x}O_4$ nanoparticles

To investigate magnetization properties of the studied nanoparticles, hysteresis loops M(H) were recorded at room temperature (Figure 3a). The found values of the coercivity, remanent magnetization and saturation magnetization using M(H) data are summarized in Table S2. Saturation magnetization (Ms) of Fe_3O_4 was found to be 77.29 emu/g with reaching maximum value for $Zn_{0.10}Fe_{2.90}O_4$ at 91.38 emu/g. The increase of Ms with respect to parent compound (x = 0) can be interpreted in terms of elimination of Fe^{3+} moment cancelling at neighbouring A and B sites, since Zn^{2+} incorporation at A sites locally cancels superexchange A–B. The reduction of Ms for $x > 0.37$ could be due to A–B interaction and the consequent takeover of the B–B when Zn^{2+} A site occupation is sufficiently high, leading to a reduced moment per unit formula. Another result shown in Figure 3a is that all of magnetization curves go through the origin of magnetization graph. This means that the synthesized NPs show superparamagnetic behaviour at room temperature because of not exhibiting hysteresis, coercivity, and remanence.

Moreover, the temperature dependence of magnetization of $Zn_xFe_{3-x}O_4$ nanoparticles with a field of H = 100 Oe under both field cooled (FC) and zero field cooled (ZFC) condition was also investigated (Figure 3b). The ZFC curves for the samples with x = 0.56 and x = 0.66 show a weak broad maximum centred at T_B~119 K and T_B~103 K. Above the blocking temperature (T_B) magnetization FC and ZFC curves reveal superparamagnetic characteristics. ZFC curve of $Zn_{0.85}Fe_{2.15}O_4$ indicates that the blocking temperature is T_B~37 K, while rest of the samples have T_B above room temperature. The effect of inclusions of nonmagnetic ions (as zinc) in spinel ferrite nanocrystals on magnetic properties has been discussed [13]. These changes in magnetic properties are probably due to an increase in the magnetic disorder induced by a decrease in the

magnetic interactions of the ions between the sublattices, which favours frustrations, i.e. changes in the orientation of individual magnetic moments.

>>> Here Figure 3<<<

The heating ability of the coated materials of $Zn_xFe_{3-x}O_4$ NPs in water suspension at physiological pH was performed to study the differences of samples morphology and crystallinity by evaluating the specific absorption rate, i.e. the absorbed power per mass unit of the water suspension. The SAR values were estimated from the initial slope of the kinetic curves, *dT/dt(0)*, using the equation 2:

$$\text{SAR (W/g)} = c_{NP} + \frac{\rho_1}{\rho_{NP}} \times c_1 \times \left(\frac{dT}{dt}\right)_{max} \quad (2)$$

where ρ_{NP} denotes density of nanoparticles in the colloid, ρ_1 density of the liquid in the colloid, $\left(\frac{dT}{dt}\right)_{max}$ maximum gradient of the temperature curve of the colloid, while c_1 and c_{NP} are specific heat of the liquid and specific heat of the nanoparticles. Figure 4 shows the differences of SAR calculated by "the slope method" (change of temperature over time for different frequencies: 252 kHz and 577 kHz) for prepared samples. The experimental kinetic curves are shown in Figure S4, while the SAR values are reported in Table S2. Pure magnetite NPs of 19.8 nm results a SAR of ~52 W/g, while measured value increases with the amount of substitution of Fe^{2+} by Zn^{2+} and the highest SAR is for $Zn_{0.37}Fe_{2.63}O_4$ of 12.8 nm with value of ~106 W/g at 252 kHz (see Table S1), which is more than twice that of pure magnetite. This demonstrates that both core sizes and chemical composition have influence in heating efficiency. The heating ability is negligible for the samples with *x* above 0.37. These results are in good arrangement with the analysis of the magnetic properties as the heating power depends on magnetization of the material, M_s.

>>> Here Figure 4<<<

Given the heterogeneity of conditions (field amplitude and frequency) for calculating SAR in different laboratories, and differences between materials (with different structure, chemical composition, shape, size etc.), it is difficult to find most appropriate examples in the literature to compare our results. For example, 10-12 nm single-domain ferrite nanoparticles coated with dextran, had a SAR value of 210 W/g (field amplitude 7.2 kA/m and frequency of 880 kHz) [50]. Our $Zn_{0.37}Fe_{2.63}O_4$ sample, with a similar particle size, presents a slightly higher SLP value (261 W/g) with the lower frequency (577 kHz) and field amplitude of 15.9 kA/m; however, the measurement conditions are not exactly the same and chemical composition is different, but it is worth noting that $Zn_{0.37}Fe_{2.63}O_4$ NPs can be used as promising candidate for the application in magnetic hyperthermia.

The intrinsic loss power (ILP) of the samples was calculated from the equation 3:

$$\text{ILP}\ (\text{nHm}^2/\text{kg}) = \frac{SAR}{H^2 f} \tag{3}$$

It ranges from 0.6 to 0.8 (in the case of samples with x = 0, 0.1 and 0.2) up to 1.7 (x = 0.37). Lastly, it must be said that field amplitude, H_0 = 15.9 kA/m and frequency, f = 252 kHz, were chosen in such manner as their product undergoes the tolerance limit ($H_0 \times f = 5 \cdot 10^9\ Am^{-1}s^{-1}$) currently accepted in order to avoid any undesired side effects on human beings for small region exposure [51]. Larger amplitudes and frequencies can induce uncontrolled tissue overheating due to generated eddy currents and peripheral stimulation of muscles. One more measurement of SAR at higher frequency, f = 577 kHz, was performed just to confirm heating ability and to emphasize differences between kinetic curves of different samples. Therefore, different heating efficiency is coming from the difference in particle size and magnetic

anisotropy, with optimum particle diameter at about 13 nm and saturation magnetisation (Ms) above 75 emu/g, induced by incorporation of zinc ions in spinel ferrite nanocrystals.

3.3. Application of $Zn_xFe_{3-x}O_4$/glassy carbon electrodes for detection of glucose

Cyclic voltammetry was applied for determination of optimum Zn level in $Zn_xFe_{3-x}O_4$ towards detection of glucose. Firstly, voltammograms were recorded in different pH of supporting electrolyte using $Zn_{0.56}Fe_{2.44}O_4$. It was found that highest response was obtained using 0.1 M NaOH as supporting electrolyte (data not shown). Similar behaviour was noticed by other authors using structurally similar nanomaterials [52,53]. Optimization of modifiers percentage wasn't done and all modifiers were tested in percentage of 5 % based on literature data and our previous experience [54,55]. Voltammograms in absence and presence of 0.01 M of glucose in 0.1 M NaOH using different modified electrodes are presented in Figure 5. As can be concluded from this study increase of Zn content in $Zn_xFe_{3-x}O_4$ up to value of x = 0.56 is followed by an increase of its possibilities toward glucose detection. These phenomena can be attributed to reduction of nanoparticles size and same trend is confirmed by previous measurements. Decrease of modified electrode characteristics is in the line with the loss of crystallinity with further increase of Zn in spinel structure. Based on these results $Zn_{0.56}Fe_{2.44}O_4$ modified glassy carbon paste electrode was selected as optimum for glucose detection.

>>> Here Figure 5<<<

Analytical characteristics of selected electrode were investigated using amperometric detection in previously found 0.1 M NaOH as supporting electrolyte at potential of 0.5 V (Figure 6). Calibration curve was constructed by plotting oxidation currents versus glucose concentrations (Inset of Figure 6). It was found that proposed non-enzymatic glucose biosensors show linear

working range from 0.1 up to 2 mM with linear regression equation, $I\ (\mu A) = 0.046\ c\ (mM) + 1.373$, and linear regression coefficient of R = 0.9941. Limit of detection (LOD) based $3\sigma_{intercept}$/slope was calculated to be 0.03 mM. Developed sensors possess comparable characteristics (limit of detection, operating range and response time) as those previously published in the literature. Characteristics of our method and some literature data are listed in Table 2. Simplicity and low-cost of material with comparable or better results, as well as easy manipulating steps and renewable electrode surface can be advantages of proposed modified carbon paste electrode. Five replicative measurements of 0.5 mM of glucose using developed method shows low RSD value of 3.4 % reflects good precision for glucose detection with negligible surface passivation.

Table 2. Comparison characteristics of developed method and some literature data

Electrode	Technique	Linear range (mM)	Detection limit (mM)	Response time (s)	Reference
ZnO nanostructure	CV	1–10	0.82	-	[56]
ZnO nanoparticles	Amperometry	1–8.6	0.000043	< 4	[57]
Pine-like Au nanostructure	Amperometry	0.02–0.24	0.00339	-	[58]
RGO/Nickel/ZnO heterostructures	Amperometry	0.0005–1.11	0.00015	< 3	[59]
$Zn_{0.56}Fe_{2.44}O_4$	Amperometry	0.1–2	0.03	< 3	*The current study*

Selectivity of developed method was tested using naturally occurring compounds such as ascorbic acid and uric acid, which can degrade efficiency of proposed sensor towards glucose determination (Figure 6b). It is expected that physiological concentration of glucose in human is about 4–7 mM and concentration of these interfering compounds is much lower (around 0.05 mM or lower). The amperometric response of developed modified electrode to sequential injection of different concentration of glucose and 0.05 mM of ascorbic and uric acids at operating potential of 0.5 V clearly indicates negligible influence of these interfering compounds and leads to the conclusion that the developed method provides considerably selective, sensitive and precise quantification of glucose.

>>>Here Figure 6<<<

3.4.Practical application of developed procedure for the determination of glucose in blood samples

Applicability of proposed method was tested for the determination of glucose level in artificial model samples. Samples were prepared following next procedure: 7 g of human serum albumin was dissolved in 100 ml physiological solution (0.9% NaCl in 0.01 M phosphate buffer at pH 7.4. Then, 5 model samples were prepared by addition of known amount of glucose. Spiked samples were in concentration of 2, 5, 7, 10 and 18 mM of glucose. The 1.0 mL of model sample solution was transferred into a volumetric flask and made up to the final volume (10 mL) with 0.1 M NaOH. Results were calculated from the calibration curves with three repetitive measurements and summarized in Table S2 (Supplementary material). A commercial glucometer (Ascenia BRIO Blutzuckerkontrol System, Bayer Healthcare) was used for the reference of glucose determination in blood. The satisfactory comparable results, using our method and

reference method, indicate that this biosensor can be successfully applied for the determination of glucose in human serum samples without matrix interferences.

4. Conclusions

Spinel structured $Zn_xFe_{3-x}O_4$ nanoparticles have been prepared and tested for potential applications in biosensors and magnetic hyperthermia. Zinc content in $Zn_xFe_{3-x}O_4$ strongly influenced characteristics of material which are essential for applications. Prepared $Zn_xFe_{3-x}O_4$/carbon paste electrodes were used for the development of new reagentless glucose sensor. The electrodes were tested toward glucose non-enzymatic detection. It can be said that synthesized $Zn_xFe_{3-x}O_4$ were exploited for the first time in connection with amperometric technique to elaborate the novel and advanced electrochemical protocols for simple, low cost and reagentless analytical determination of glucose. On the other side, substituted zinc ferrite nanoparticles have potential as heating agents in magnetic hyperthermia application. The Zn content of $x = 0.56$ ($Zn_{0.56}Fe_{2.44}O_4$) were found as optimum for modification of carbon electrodes application, while the highest SAR value was calculated for $x = 0.37$ ($Zn_{0.37}Fe_{2.63}O_4$).

Acknowledgment

This work was supported by the Ministry of Education, Science and Technological Development of the Republic of Serbia through the Eureka Project, E!9982. MO, DMS and Z.P. were supported by the European Commission through the Project MagBioVin, Grant agreement #621375.

References

[1] C. Yao, Q. Zeng, G.F. Goya, T. Torres, J. Liu, H. Wu, M. Ge, Y. Zeng, Y. Wang, J.Z. Jiang, ZnFe2O4 Nanocrystals: Synthesis and Magnetic Properties, J. Phys. Chem. C 111 (33) (2007) 12274–12278.

[2] D.S. Mathew, R.-S. Juang, An overview of the structure and magnetism of spinel ferrite nanoparticles and their synthesis in microemulsions, Chem. Eng. J. 129 (1-3) (2007) 51–65.

[3] M. Sultan, R. Singh, Structural and optical properties of RF-sputtered $ZnFe_2O_4$ thin films, J. Phys. D. 42 (11) (2009) 115306.

[4] Y.F. Chen, D. Spoddig, M. Ziese, Epitaxial thin film ZnFe2O4: A semi-transparent magnetic semiconductor with high Curie temperature, J. Phys. D. 41 (20) (2008) 205004.

[5] C. Xavier, R. Candeia, M. Bernardi, S. Lima, E. Longo, C. Paskocimas, L. Soledade, A. Souza, I. Santos, Effect of the modifier ion on the properties of $MgFe_2O_4$ and $ZnFe_2O_4$ pigments, J. Therm. Anal. Calorim. 87 (3) (2007) 709–713.

[6] H. Lee, J.C. Jung, H. Kim, Y.-M. Chung, T.J. Kim, S.J. Lee, S.-H. Oh, Y.S. Kim, I.K. Song, Preparation of $ZnFe_2O_4$ catalysts by a co-precipitation method using aqueous buffer solution and their catalytic activity for oxidative dehydrogenation of n-butene to 1,3-butadiene, Catal. Lett. 122 (3-4) (2008) 281–286.

[7] J.A. Toledo-Antonio, N. Nava, M. Martınez, X. Bokhimi, Correlation between the magnetism of non-stoichiometric zinc ferrites and their catalytic activity for oxidative dehydrogenation of 1-butene, App. Catal. A: General 234 (1) (2002) 137–144.

[8] J. Jang, H. Nah, J. Lee, S.H. Moon, M.G. Kim, J. Cheon, Critical Enhancements of MRI Contrast and Hyperthermic Effects by Dopant□Controlled Magnetic Nanoparticles, Angew. Chem. 121 (7) (2009) 1260–1264.

[9] P. Majewski, B. Thierry, Functionalized Magnetite Nanoparticles-Synthesis, Properties, and Bio-Applications, Crit. Rev. Solid State Mater. Sci. 32 (3-4) (2007) 203–215.

[10] J.S. Kim, T.-J. Yoon, K.N. Yu, B.G. Kim, S.J. Park, H.W. Kim, K.H. Lee, S.B. Park, J.-K. Lee, M.H. Cho, Toxicity and tissue distribution of magnetic nanoparticles in mice, Toxicol. Sci. 89 (1) (2006) 338–347.

[11] P. Tartaj, S. Veintemillas-Verdaguer, C.J. Serna, The preparation of magnetic nanoparticles for applications in biomedicine, J. Phys. D: Appl. Phys. 36 (13) (2003) R182.

[12] H.S. Nalwa, Encyclopedia of Nanoscience and Nanotechnology; Volume 7, American Scientific Publishers, 2004.

[13] J.F. Hochepied, P. Bonville, M.P. Pileni, Nonstoichiometric Zinc Ferrite Nanocrystals: Syntheses and Unusual Magnetic Properties, J. Phys. Chem. B 104 (5) (2000) 905–912.

[14] A.H. Morrish, Z.W. LI, J.Z. Jiang, magnetic structure of zinc-ferrite approaching nanometer sizes, Int. J. Mod. Phys. B 15 (24n25) (2001) 3312–3316.

[15] C. Pereira, A.M. Pereira, C. Fernandes, M. Rocha, R. Mendes, M.P. Fernández-García, A. Guedes, P.B. Tavares, J.-M. Grenèche, J.P. Araújo, C. Freire, Superparamagnetic MFe_2O_4 (M = Fe, Co, Mn) Nanoparticles: Tuning the Particle Size and Magnetic Properties through a Novel One-Step Coprecipitation Route, Chem. Mater. 24 (8) (2012) 1496–1504.

[16] M. George, A. Mary John, S.S. Nair, P.A. Joy, M.R. Anantharaman, Finite size effects on the structural and magnetic properties of sol–gel synthesized $NiFe_2O_4$ powders, J. Magn. Magn. Mater. 302 (1) (2006) 190–195.

[17] E. Mazario, M.P. Morales, R. Galindo, P. Herrasti, N. Menendez, Influence of the temperature in the electrochemical synthesis of cobalt ferrites nanoparticles, J. Alloys Compd. 536 (2012) S222-S225.

[18] C. Liu, A.J. Rondinone, Z.J. Zhang, Synthesis of magnetic spinel ferrite $CoFe_2O_4$ nanoparticles from ferric salt and characterization of the size-dependent superparamagnetic properties, Pure Appl. Chem. 72 (1-2) (2000).

[19] E. Manova, B. Kunev, D. Paneva, I. Mitov, L. Petrov, C. Estournès, C. D'Orléan, J.-L. Rehspringer, M. Kurmoo, Mechano-Synthesis, Characterization, and Magnetic Properties of Nanoparticles of Cobalt Ferrite, $CoFe_2O_4$, Chem. Mater. 16 (26) (2004) 5689–5696.

[20] W. Li, X. Qiao, Q. Zheng, T. Zhang, One-step synthesis of MFe_2O_4 (M=Fe, Co) hollow spheres by template-free solvothermal method, J. Alloys Compd. 509 (21) (2011) 6206–6211.

[21] W. Hu, N. Qin, G. Wu, Y. Lin, S. Li, D. Bao, Opportunity of spinel ferrite materials in nonvolatile memory device applications based on their resistive switching performances, J. Am. Chem. Soc. 134 (36) (2012) 14658–14661.

[22] X. Hu, J.C. Yu, J. Gong, Q. Li, G. Li, α-Fe2O3 Nanorings Prepared by a Microwave-Assisted Hydrothermal Process and Their Sensing Properties, Adv. Mater. 19 (17) (2007) 2324–2329.

[23] X. Hu, J.C. Yu, Continuous Aspect-Ratio Tuning and Fine Shape Control of Monodisperseα-Fe2O3 Nanocrystals by a Programmed Microwave–Hydrothermal Method, Adv. Funct. Mater. 18 (6) (2008) 880–887.

[24] Z. Ai, K. Deng, Q. Wan, L. Zhang, S. Lee, Facile Microwave-Assisted Synthesis and Magnetic and Gas Sensing Properties of Fe_3O_4 Nanoroses, J. Phys. Chem. C 114 (14) (2010) 6237–6242.

[25] S. Verma, P.A. Joy, Y.B. Khollam, H.S. Potdar, S.B. Deshpande, Synthesis of nanosized $MgFe_2O_4$ powders by microwave hydrothermal method, Mater. Lett. 58 (6) (2004) 1092–1095.

[26] G.B. Ji, S.L. Tang, S.K. Ren, F.M. Zhang, B.X. Gu, Y.W. Du, Simplified synthesis of single-crystalline magnetic $CoFe_2O_4$ nanorods by a surfactant-assisted hydrothermal process, J. Cryst. Growth 270 (1-2) (2004) 156–161.

[27] A. Baykal, N. Kasapoğlu, Y. Köseoğlu, M.S. Toprak, H. Bayrakdar, CTAB-assisted hydrothermal synthesis of $NiFe_2O_4$ and its magnetic characterization, J. Alloys Compd. 464 (1-2) (2008) 514–518.

[28] Y. Zhang, Y. Liu, L. Su, Z. Zhang, D. Huo, C. Hou, Y. Lei, CuO nanowires based sensitive and selective non-enzymatic glucose detection, Sens. Actuators B Chem. 191 (2014) 86–93.

[29] E.-H. Yoo, S.-Y. Lee, Glucose biosensors: an overview of use in clinical practice, Sensors (Basel, Switzerland) 10 (5) (2010) 4558–4576.

[30] K. Tian, M. Prestgard, A. Tiwari, A review of recent advances in nonenzymatic glucose sensors, Mater. Sci. Eng. C Mater. Biol. Appl. 41 (2014) 100–118.

[31] S.P. Nichols, A. Koh, W.L. Storm, J.H. Shin, M.H. Schoenfisch, Biocompatible materials for continuous glucose monitoring devices, Chem. Rev. 113 (4) (2013) 2528–2549.

[32] M.M. Rahman, A.J.S. Ahammad, J.-H. Jin, S.J. Ahn, J.-J. Lee, A comprehensive review of glucose biosensors based on nanostructured metal-oxides, Sensors (Basel, Switzerland) 10 (5) (2010) 4855–4886.

[33] Y. Xian, Y. Hu, F. Liu, Y. Xian, H. Wang, L. Jin, Glucose biosensor based on Au nanoparticles-conductive polyaniline nanocomposite, Biosens. Bioelectron. 21 (10) (2006) 1996–2000.

[34] S. Park, T.D. Chung, H.C. Kim, Nonenzymatic Glucose Detection Using Mesoporous Platinum, Anal. Chem. 75 (13) (2003) 3046–3049.

[35] F. Xiao, F. Zhao, D. Mei, Z. Mo, B. Zeng, Nonenzymatic glucose sensor based on ultrasonic-electrodeposition of bimetallic PtM (M=Ru, Pd and Au) nanoparticles on carbon nanotubes-ionic liquid composite film, Biosens. Bioelectron. 24 (12) (2009) 3481–3486.

[36] I.-H. Yeo, D.C. Johnson, Electrochemical response of small organic molecules at nickel–copper alloy electrodes, J. Electroanal. Chem. 495 (2) (2001) 110–119.

[37] B. Singh, F. Laffir, T. McCormac, E. Dempsey, PtAu/C based bimetallic nanocomposites for non-enzymatic electrochemical glucose detection, Sens. Actuators B Chem. 150 (1) (2010) 80–92.

[38] J. Wang, D.F. Thomas, A. Chen, Nonenzymatic electrochemical glucose sensor based on nanoporous PtPb networks, Anal. Chem. 80 (4) (2008) 997–1004.

[39] Z. Shahnavaz, P.M. Woi, Y. Alias, Electrochemical sensing of glucose by reduced graphene oxide-zinc ferrospinels, Appl. Surf. Sci. 379 (2016) 156–162.

[40] A.M. Abdul Amir AL-Mokaram, R. Yahya, M.M. Abdi, H.N. Muhammad Ekramul Mahmud, One-step electrochemical deposition of Polypyrrole–Chitosan–Iron oxide nanocomposite films for non-enzymatic glucose biosensor, Mater. Lett. 183 (2016) 90–93.

[41] H.A. Wahab, A.A. Salama, A.A. El Saeid, M. Willander, O. Nur, I.K. Battisha, Zinc oxide nano-rods based glucose biosensor devices fabrication, Results in Phys. 9 (2018) 809-814.

[42] M. Marie, S. Mandal, O. Manasreh, An electrochemical glucose sensor based on zinc oxide nanorods. Sensors, 15(8) (2015), 18714-18723.

[43] M. Ognjanović, B. Dojčinović, M. Fabián, D.M. Stanković, J.F. Mariano, B. Antić, Microwave assisted hydrothermal synthesis of $(Fe,Co)_3O_4$ nanoparticles in the presence of

surfactants and effects of Co/Fe ratio on microstructure and magnetism, Ceram. Int. 44 (12) (2018) 13967-13972.

[44] H.P. Klug, L.E. Alexander, X-ray diffraction procedures (1954).

[45] L. Vegard, Die konstitution der mischkristalle und die raumfüllung der atome, Zeitschrift für Physik 5 (1) (1921) 17–26.

[46] C. Rath, S. Anand, R.P. Das, K.K. Sahu, S.D. Kulkarni, S.K. Date, N.C. Mishra, Dependence on cation distribution of particle size, lattice parameter, and magnetic properties in nanosize Mn–Zn ferrite, J. Appl. Phys. 91 (4) (2002) 2211–2215.

[47] R.D. Shannon, Revised effective ionic radii and systematic studies of interatomic distances in halides and chalcogenides, Acta Cryst. A 32 (5) (1976) 751–767.

[48] J. Liu, Y. Bin, M. Matsuo, Magnetic Behavior of Zn-Doped Fe 3 O 4 Nanoparticles Estimated in Terms of Crystal Domain Size, J. Phys. Chem. C 116 (1) (2012) 134–143.

[49] W.B. White, B.A. DeAngelis, Interpretation of the vibrational spectra of spinels, Spectrochim. Acta A: Molecular Spectroscopy 23 (4) (1967) 985–995.

[50] S. Mornet, S. Vasseur, F. Grasset, E. Duguet, Magnetic nanoparticle design for medical diagnosis and therapy, J. Mater. Chem. 14 (14) (2004) 2161.

[51] W.J. Atkinson, I.A. Brezovich, D.P. Chakraborty, Usable frequencies in hyperthermia with thermal seeds, IEEE transactions on bio-medical engineering 31 (1) (1984) 70-75.

[52] S.Y. Tee, C.P. Teng, E. Ye, Metal nanostructures for non-enzymatic glucose sensing, Mater. Sci. Eng. C Mater. Biol. Appl. 70 (Pt 2) (2017) 1018–1030.

[53] C.-W. Hsu, F.-C. Su, P.-Y. Peng, H.-T. Young, S. Liao, G.-J. Wang, Highly sensitive non-enzymatic electrochemical glucose biosensor using a photolithography fabricated micro/nano hybrid structured electrode, Sens. Actuators B Chem. 230 (2016) 559–565.

[54] S. Škrivanj, D.M. Stanković, M. Khan, A.S. Nikolić, P. Vulić, D.D. Manojlović, Sensitive determination of copper on new modified glassy carbon paste electrode, Anal. Bioanal. Electrochem. 7 (2015) 230–241.

[55] D.M. Stanković, S. Škrivanj, N. Savić, A.S. Nikolić, P. Vulić, D.D. Manojlović, Application of Novel Zn-Ferrite Modified Glassy Carbon Paste Electrode as a Sensor for Determination of Cd(II) in Waste Water, Electroanalysis 26 (7) (2014) 1536–1543.

[56] A. Tarlani, M. Fallah, B. Lotfi, A. Khazraei, S. Golsanamlou, J. Muzart, M. Mirza-Aghayan, New ZnO nanostructures as non-enzymatic glucose biosensors, Biosens. Bioelectron. 67 (2015) 601–607.

[57] T. Dayakar., K. Venkateswara Rao., K. Bikshalu., V. Rajendar., S.-H. Park, Novel synthesis and structural analysis of zinc oxide nanoparticles for the non enzymatic glucose biosensor, Mater. Sci. Eng. C Mater. Biol. Appl. 75 (Supplement C) (2017) 1472–1479.

[58] H. Heli, O. Amirizadeh, Non-enzymatic glucose biosensor based on hyperbranched pine-like gold nanostructure, Mater. Sci. Eng. C Mater. Biol. Appl. 63 (2016) 150–154.

[59] M. Mazaheri, H. Aashuri, A. Simchi, Three-dimensional hybrid graphene/nickel electrodes on zinc oxide nanorod arrays as non-enzymatic glucose biosensors, Sens. and Actuators B: Chem. 251 (2017) 462–471.

Figure captions:

Figure 1. (a) XRD patterns of $Zn_xFe_{3-x}O_4$ (x = 0, 0.10, 0.20, 0.37, 0.56, 0.66 and 0.85) obtained by the CuKα source-equipped diffractometer; (b) lattice parameter as a function of the zinc content x. Inset of Figure 1b represents shift of the (311) reflection peak.

Figure 2. TEM micrography of $Zn_xFe_{3-x}O_4$ nanoparticles and the particle size distribution histograms with x content of (a) 0; (b) 0.10; (c) 0.20 and (d) 0.37.

Figure 3. Magnetic characterization of $Zn_xFe_{3-x}O_4$. (a) Room temperature hysteresis loops of $Zn_xFe_{3-x}O_4$ nanoparticles with different Zn content. (b) Temperature dependence of the zero-field-cooled (ZFC) and the field-cooled (FC) magnetization measured in a field of 100 Oe.

Figure 4. SAR values of samples with different Zn content. SAR values of different samples calculated by the slope method. The field amplitude was 15.9 kA/m and two different frequencies were applied: 252 and 577 kHz.

Figure 5. (a) Cyclic voltammograms in presence and absence of 0.01 M of glucose using $Zn_xFe_{3-x}O_4$ (with x = 0, 0.10, 0.20, 0.37, 0.56, 0.66 and 0.85) modified glassy carbon paste electrode in 0.1 M NaOH supporting electrolyte. (b) Cyclic voltammograms in presence of 0.1 M of glucose using $Zn_{0.56}Fe_{2.44}O_4$ modified glassy carbon paste electrode in 0.1 M NaOH as supporting electrolyte.

Figure 6. (a) Amperometric detection of glucose using $Zn_{0.56}Fe_{2.44}O_4$ modified glassy carbon paste electrode. Inset figure represents corresponding calibration curve. (b) Amperometric detection of glucose using $Zn_{0.56}Fe_{2.44}O_4$ modified glassy carbon paste electrode in presence of ascorbic acid and uric acid at concentration level of 0.05 mM. Supporting electrolyte was 0.1 M NaOH at working potential of 0.5 V.

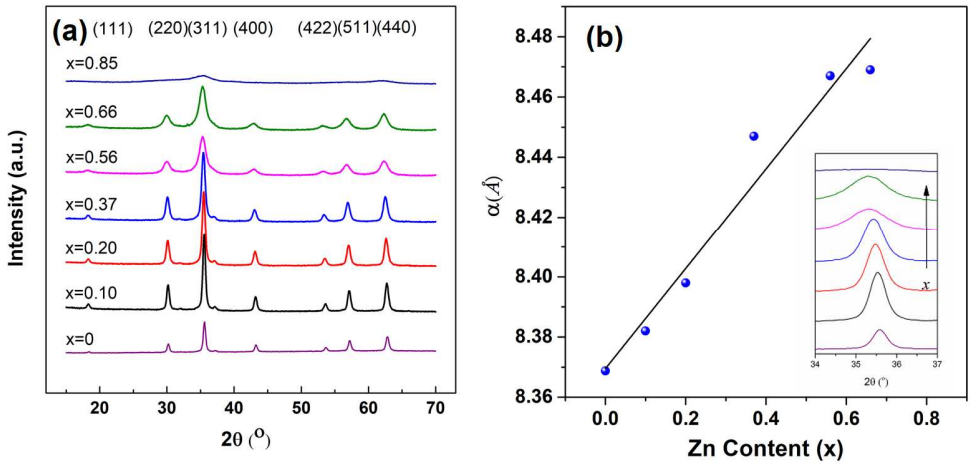

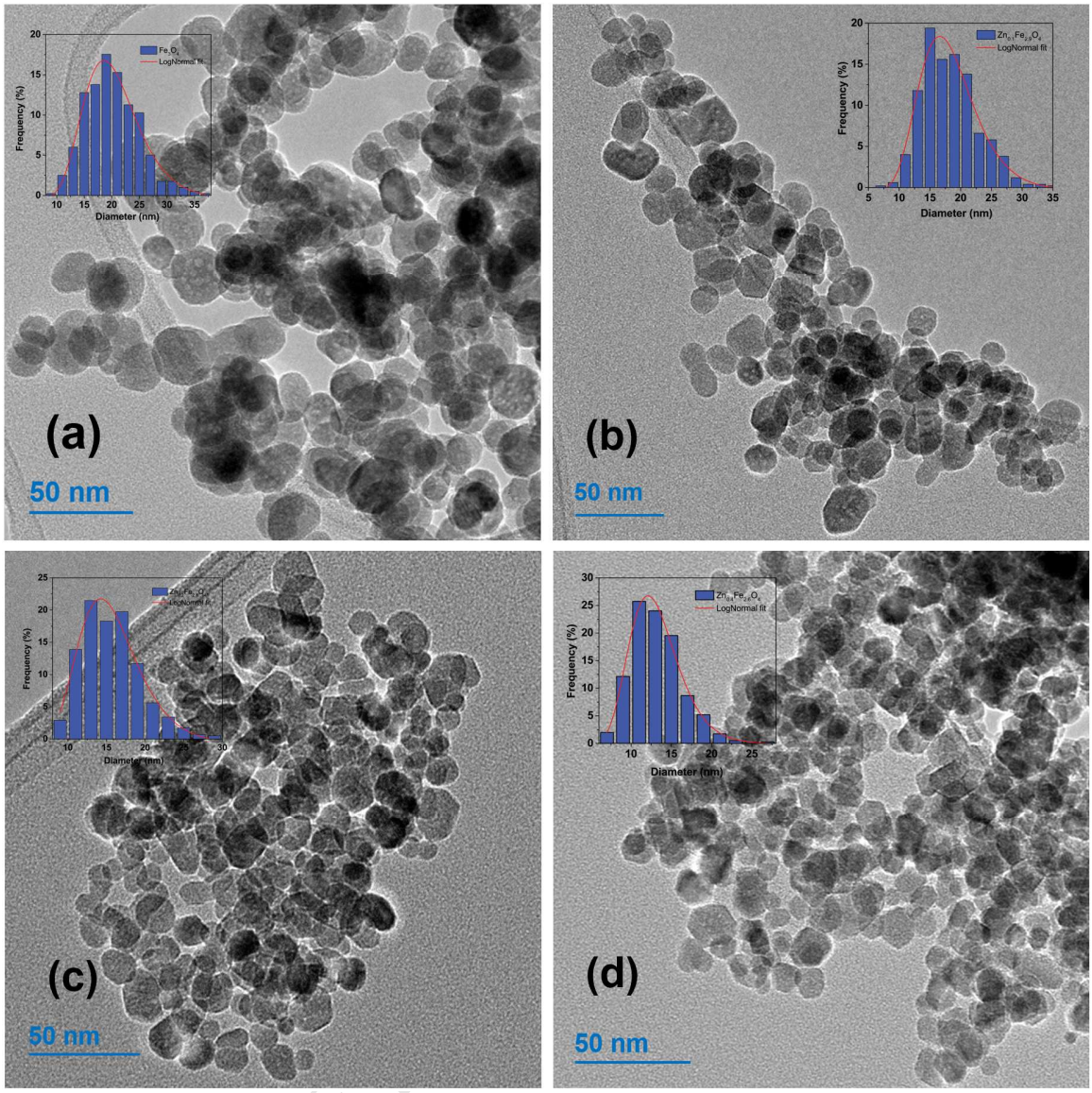
(a)
50 nm
Frequency (%)
Diameter (nm)
LogNormal fit
(b)
50 nm
Frequency (%)
Diameter (nm)
LogNormal fit
(c)
50 nm
Frequency (%)
Diameter (nm)
(d)
50 nm
Frequency (%)
Diameter (nm)
LogNormal fit

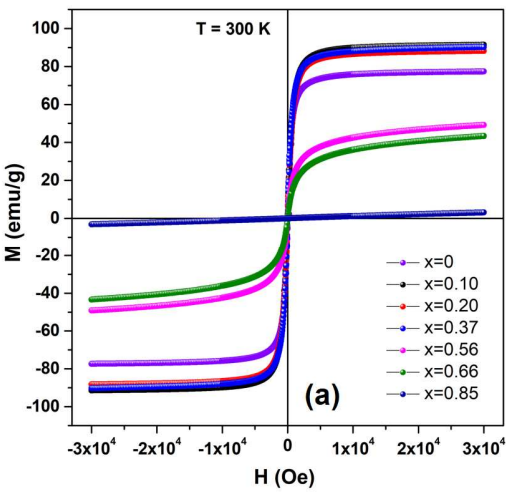

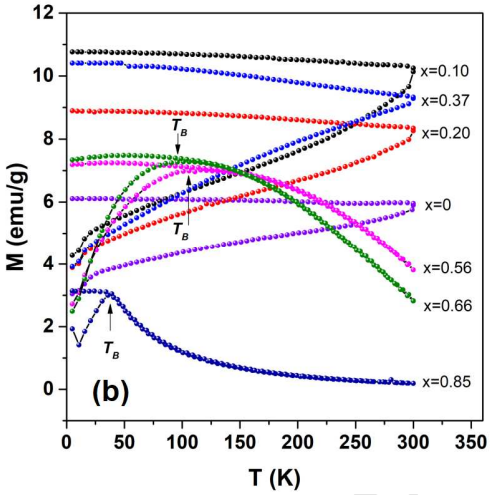

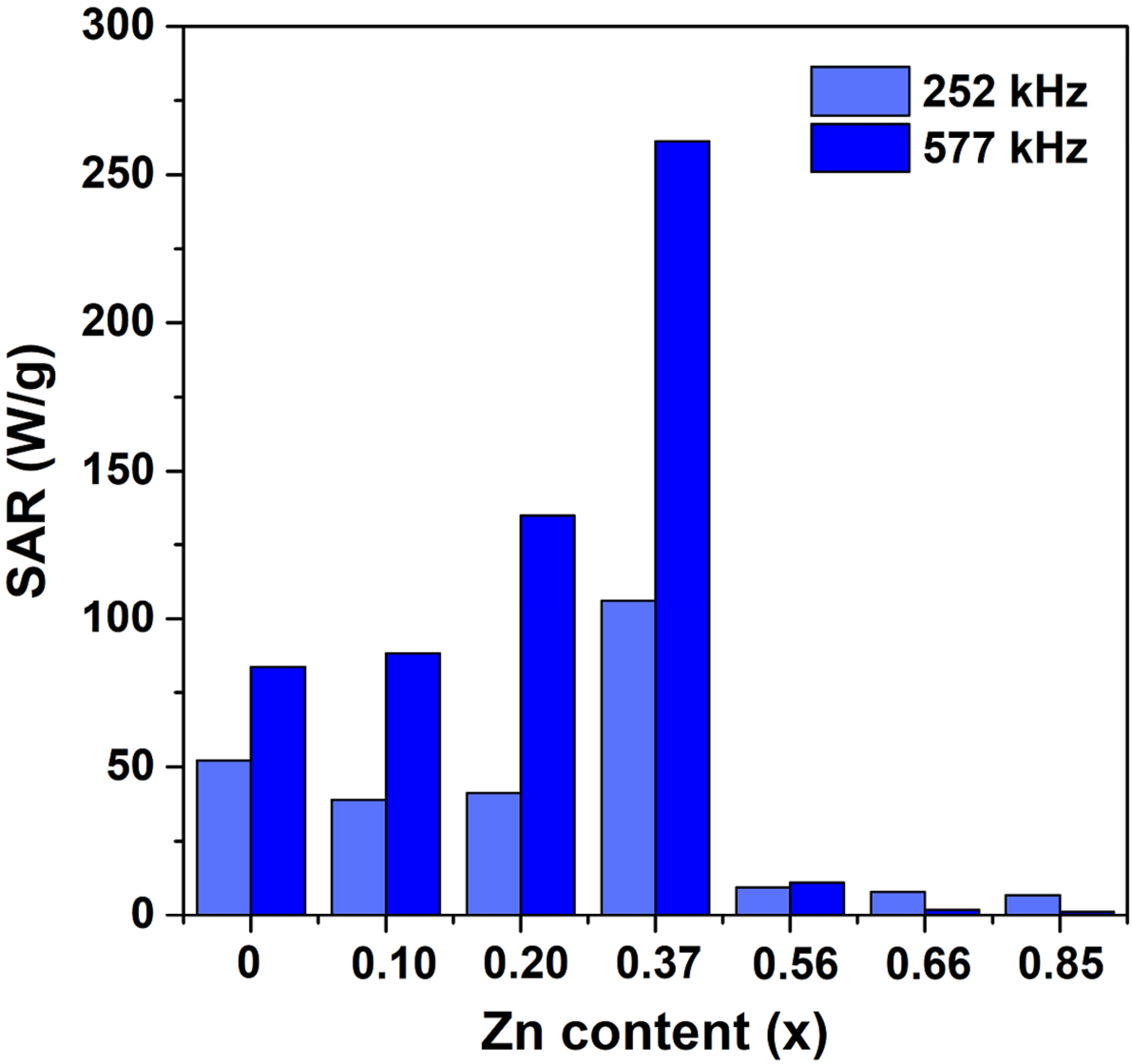
300
250
200
150
100
50
0
SAR (W/g)
252 kHz
577 kHz
0
0.10
0.20
0.37
0.56
0.66
0.85
Zn content (x)

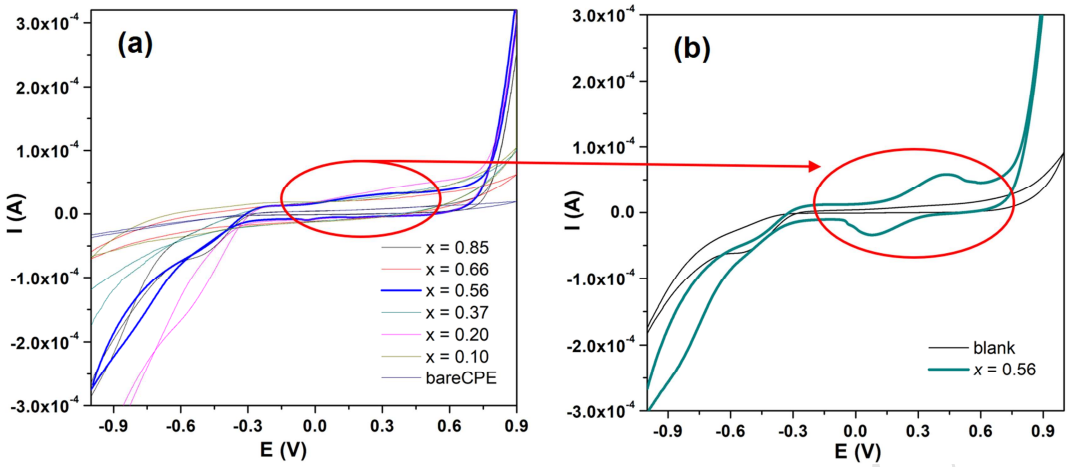

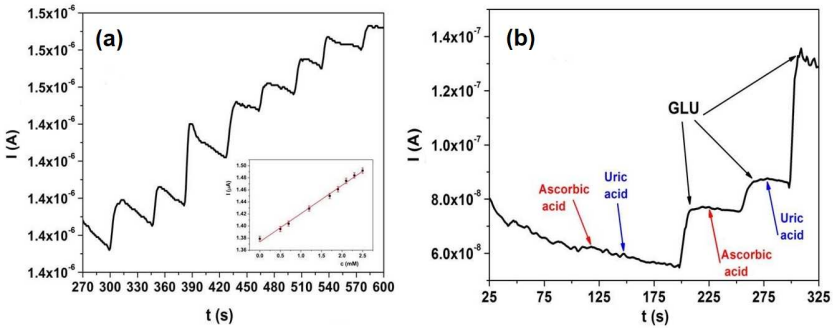

Highlights:

- Preparation of $Zn_xFe_{3-x}O_4$ composite by co-precipitation method in combination with hydrothermal treatment.
- Effect of zinc content in ferrite structure was investigated and bifunctionality of the material was shown.
- Construction of non-enzymatic glucose biosensor based on substituted magnetite was done.
- Promising sensitivity, satisfactory selectivity and simplicity of glucose detection were achieved.
- Prepared materials were tested as potential heating agents in magnetic hyperthermia.